JOURNAL OF MATERIALS SCIENCE 37 (2002) 1869–1873

Fatigue and R-curve behavior of an Al_2O_3-10vol%Cr_3C_2 composite

CHING-AN JENG, JOW-LAY HUANG, SHI-MIN WANG, CHING-YUN CHEN
Department of Materials Science and Engineering, National Cheng-Kung University, Tainan, Taiwan 701, ROC
E-mail: JLH888@mail.ncku.edu.tw

The static and dynamic fatigue properties of an Al_2O_3-10 composite were studied. The R-Curve behavior was determined using the indentation strength in bending (ISB) technique. Results indicated that both alumina and the Al_2O_3-Cr_3C_2 composite exhibit time-dependent slow crack growth under static fatigue test conditions. In addition, the resistance for slow crack growth in the Al_2O_3-Cr_3C_2 composite is higher than that in monolithic alumina. The toughness of alumina was substantially increased and R-curve behavior became evident after the incorporation of Cr_3C_2 particles.

1. Introduction

Alumina has been widely used because of its good mechanical properties, chemical stability and high temperature characteristics. However, its intrinsic brittleness and relatively poor reliability have made the toughening of alumina ceramics essential but challenging. Among the reported toughening methods, hard particulate reinforcement has been found to be an easy, safe, efficient and economical technique [1–5].

Chromium carbide has been successfully incorporated into Al_2O_3 [6–8] and TiB_2 [9] for toughening purpose, owing to its high Young's modulus and high-temperature erosion resistance. In addition, the high electrical conductivity of Cr_3C_2 has made electrical discharge machining of alumina composites possible [10].

The effects of sintering atmosphere, phase stability and microstructure on the mechanical properties and crack behaviors of the resulting Al_2O_3/Cr_3C_2 composite have been discussed in earlier studies [5, 11]. In this paper, the static and dynamic fatigue properties of an Al_2O_3-10vol%Cr_3C_2 composite were examined. The R-Curve behavior was determined from indentation strength in bending (ISB) technique.

2. Experimental procedure

2.1. Sample preparation

Alumina powder (Alcoa A16-SG, 0.6 μm) was mixed with 10 vol% chromium carbide (Herman C. Starck 160, 2 μm) in a polyurethane bottle with high purity alumina balls and ethanol for 24 h. The ratio of charge to vehicle to ball was 1 : 5 : 6 by mass. The slurry was then dried in a rotating vacuum condensor, ground with an alumina mortar and pestle, and passed through a 100 mesh screen to break up agglomerates.

Injection molding was used to fabricate test samples. The binders used in this study included paraffin wax (PW), polypropylene (PP) and steric acid (SA) with a ratio of 65 : 30 : 5 by mass. Blending and pelletization were conducted in a two blade mixer (Irie Shokai Co., Japan, PN-1H) at 190°C and 60 rpm.

The barrel temperatures for injection moulding were in the range of 150–160°C (from feeder to nozzle). The injection pressure and rate were 70 MPa and 40 ml s^{-1} respectively. Samples were first immersed in n-heptane at 90°C for 1 h to extract the binders then rinsed in alcohol before thermal debinding. Samples were placed on alumina powder for thermal debinding up to 500°C in air, cold isostatically pressed at 100 MPa, then sintered in a powder bed of the same composition in a graphite furnace (Centorr/Vacuum Industries, Inc., USA, model 10-2) at 1550°C for 2 h. The average sintered density was more than 98.5% of the theoretical density. Some physical and mechanical properties of the Al_2O_3 and the Al_2O_3-Cr_3C_2 composite are shown in Table I.

2.2. Static fatigue test

Samples with dimensions of 3 × 4 × 50 mm were polished to 1 μm finish. An indentation impression was made on a polished surface using a diamond Vickers Indenter (AKASHI AVK-A) at 49N for 15 s. Specimens were then annealed at 800°C for 2 h to relieve the residual stresses before undergoing a four-point bending fatigue test. The outer and inner spans used were 40 and 20 mm respectively.

2.3. Dynamic fatigue test

Specimens were prepared in the same way as those used for the static fatigue test and tested in water. The dynamic fatigue test was conducted under various loading rates, i.e., 0.34, 3.34, 34.4, and 344 MPa/sec. The outer and inner spans were the same as used in the static fatigue test.

TABLE I Physical and mechanical properties of Al_2O_3 and 10%Cr_3C_2-Al_2O_3 composite

Properties	Al_2O_3	10%Cr_3C_2-Al_2O_3 composite
Density (g/cm^3)	3.85	4.10
Grain size (μm)	4–6	3–4
Hardness (GPa)	15	16.8
RT flexural strength (MPa)	380	495
Youngs' modulus (GPa)	360	365
Poisson ratio	0.21	0.24
Fracture toughness (MPa/m$^{-1/2}$)	4.2	5.1

2.4. R-curve behavior

2.4.1. Indentation strength in bending (ISB)

R-curve behavior was investigated by expressing the fracture resistance K_R as a function of crack extension (Δc) in response to a fractional power:

$$K_R = A(\Delta c)^n \tag{1}$$

where A and n are parameters which could be determined from the following equations [12, 13]:

$$\log \sigma = \log \alpha + \beta \log P \tag{2}$$

$$\alpha = [A\pi^{1/2}(3+2n)/8\Omega] \bullet [4(\chi/A)/(1-2n)]^{(2n-1)/(2n+3)} \tag{3}$$

$$\beta = (2n-1)/(2n+3) \tag{4}$$

$$c = [P\chi/A]^{2/(3+2n)} \tag{5}$$

c and σ are crack length and flexural strength respectively at applied indentation load P; Ω is a crack geometry parameter which can be determined from the ratios of crack length to sample dimensions following an empirical equation derived by Newman and Raju [14], and χ is a dimensionless constant which is characteristic of the material and indentor geometry. In general, the crack extension, $\Delta c = c - c_N$, applies to stressed crack surfaces, c_N being a stress-free notch. The c_N is considered to be zero in the ISB.

A varying flaw size, controlled by Vickers indentation loading (P) from 49 to 490 N, was placed on the prospective tensile surfaces of the specimens. The length of surface cracks (c) was measured by optical microscopy. An universal testing machine (Instron 8511) was used to produce the loading stress (σ) required to rupture a specimen under four-point bending.

Parameters n and A in (1) could be determined from Equations 2 to 5 according to the relationship between the crack length, corresponding fracture load and the applied indentation load [13].

2.4.2. Dummy-indentation method

A modified ISB indentation technique developed by Cook and Lawn [15, 16] was used to estimate the R-curve behavior using indentation-produced flaws. The sample preparation was the same as that of the ISB method except that three indentations made under the same applied load were placed in the middle of the prospective tensile surface prior to bend test. The surface indentations were introduced at 98, 196, 294 and 490 N for 15 sec using a Vickers indentor. Samples were immediately fractured after indentation to avoid slow crack propagation. Failure occurs from just one of the three indentations, leaving intact dummies available for the measurement of critical crack dimensions. The stress intensity factor (K_R) can therefore be calculated from the crack subjected to an applied stress (σ).

$$K_R(c_I) = \chi P/c_I^{3/2} \tag{6}$$

$$K_R(c_T) = 2\Omega\sigma(c_T/\pi)^{1/2} + \chi P/c_T^{3/2} \tag{7}$$

where Ω is a crack geometry parameter as defined in Equation 3 [14], c_I is the initial crack length at a given indentation load, and c_T is the critical crack length determined from the dummies after the bend test. The parameter χ is a dimensionless indenter-material constant [17–20]. P is the applied indentation load.

3. Results and discussion

3.1. Dynamic fatigue

The strength of Al_2O_3 and the Al_2O_3-Cr_3C_2 composite were determined as a function of loading rate as shown in Fig. 1. It is evident that the addition of Cr_3C_2 to Al_2O_3 significantly improves the strength. In addition, the strength of both materials increases with the stressing rate. The slopes in Fig. 1 can be expressed as $1/(N+1)$, where N is the crack-growth velocity exponent [21–23]. The corresponding N-values for Al_2O_3 and Al_2O_3-Cr_3C_2 are calculated to be 47 and 63 respectively. The higher value of N for the Al_2O_3-Cr_3C_2 material indicates that it has a higher resistance to slow crack growth than monolithic alumina [24]. Fig. 2 shows a typical fractured surface of the Al_2O_3-Cr_3C_2 composite after a dynamic test at a stressing rate of 0.34 MPa/s. There was no obvious difference between the indentation precracked zone and the fast fracture zone. An intergranular fracture region was observed just outside the indentation precrack zone, as shown in Fig. 2b.

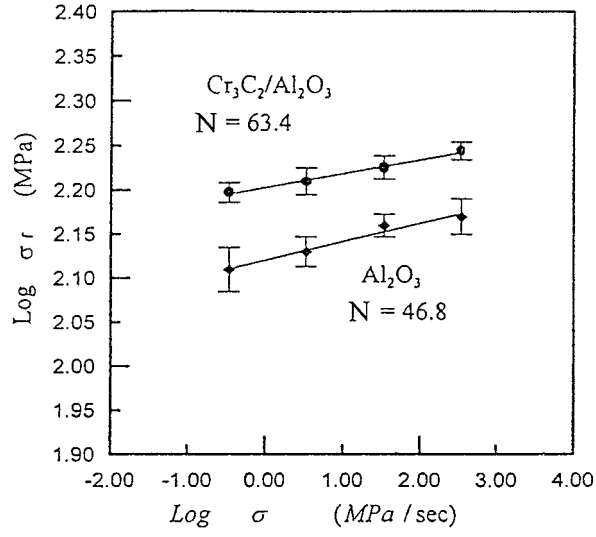

Figure 1 Dynamic fatigue results of alumina and Al_2O_3-Cr_3C_2 composite. Samples were tested at room temperature in water.

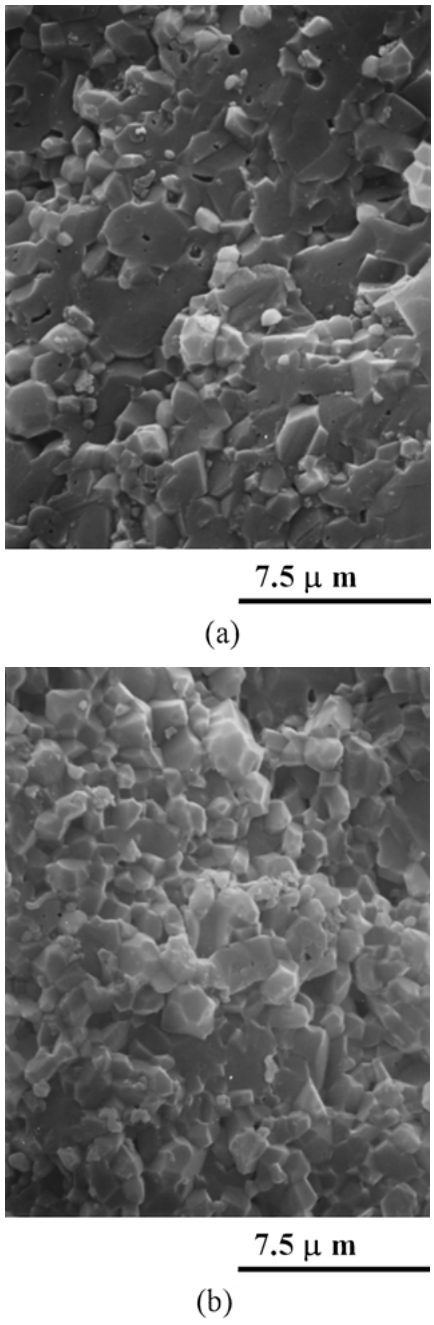

Figure 2 Fracture surfaces of a Al_2O_3-Cr_3C_2 composite sample after testing in dynamic fatigue at a stressing rate of 0.34 MPa/s: (a) precrack zone (fast fracture zone) and (b) a region away from the precrack zone.

3.2. Static fatigue

The applied stress versus failure time for both Al_2O_3 and the Al_2O_3-Cr_3C_2 composite is shown in Fig. 3. A correlation between the applied load (σ), failure time (t), and slow crack growth parameter (N) can be expressed as $\ln \sigma = A \cdot (\ln t)^{-(1/N)}$ where A is a constant [25]. The slow crack growth parameter N can therefore be calculated from the slopes in Fig. 3. The calculated N values are 51 and 61 for monolithic alumina and Al_2O_3-Cr_3C_2, respectively. These values are in good agreement with those of dynamic test results shown in Fig. 1.

The average slow crack velocity (V) can be expressed as a power function of the stress intensity factor $V(K_I) = A(K_I)^N$, where A and N are constants dependent on environment and type of material. A Plot of

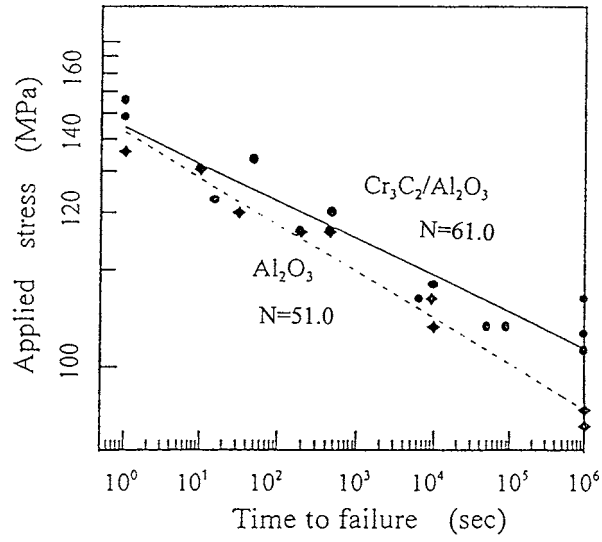

Figure 3 Static fatigue results of alumina and the Al_2O_3-Cr_3C_2 composite. Samples were tested at room temperature in water.

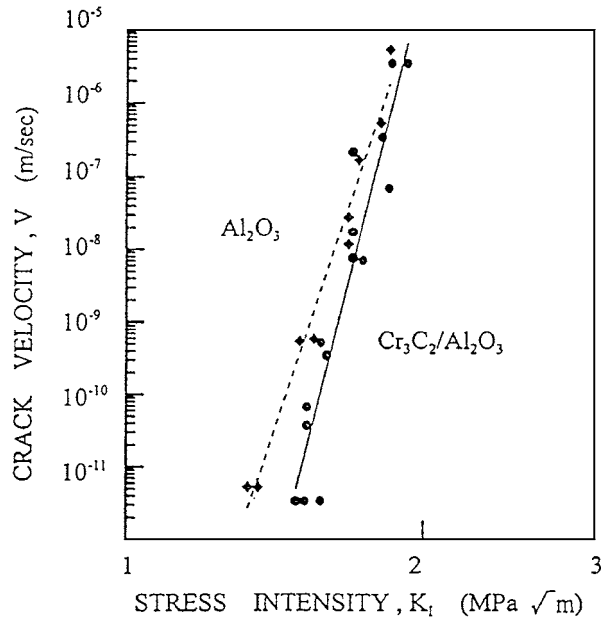

Figure 4 Crack growth velocity versus stress intensity factor.

crack velocity versus stress intensity factor is shown in Fig. 4. The results suggest that subcritical crack growth is hindered by the incorporation of Cr_3C_2 particulates. Similar observations were reported for Y-TZP and alumina-toughened Y-TZP materials [26].

3.3. R-curve behavior

3.3.1. Dummy-indentation method

The stress intensity factors for the initial crack length $K_R(c_I)$ are calculated from Equation 6, the values being shown by the solid squares in Fig. 5. Fracture toughness values, determined from dummys indentations, according to Equation 7 are also plotted in the same figure (open squares). χ in Equation 7 can be calculated from the applied load and indentation crack length [20, 27, 28]. Ω can be calculated from the sample width and crack depth [14, 29]. An empirical equation involving the upper-bound and lower-bound fracture

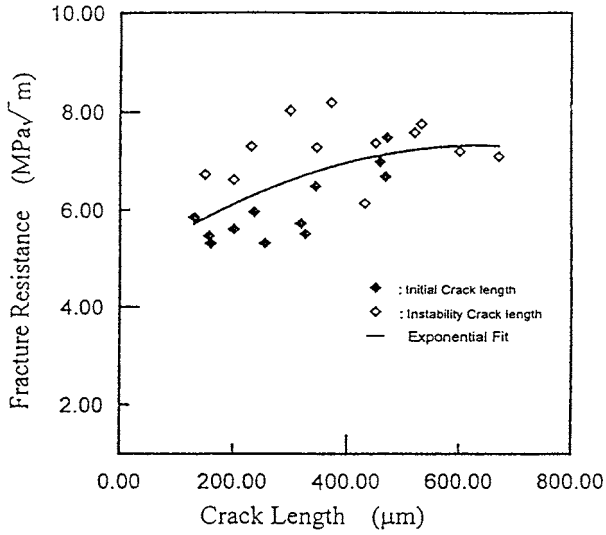

Figure 5 Rising crack-growth resistance of Al_2O_3-Cr_3C_2 composites determined by the dummy-indentation method.

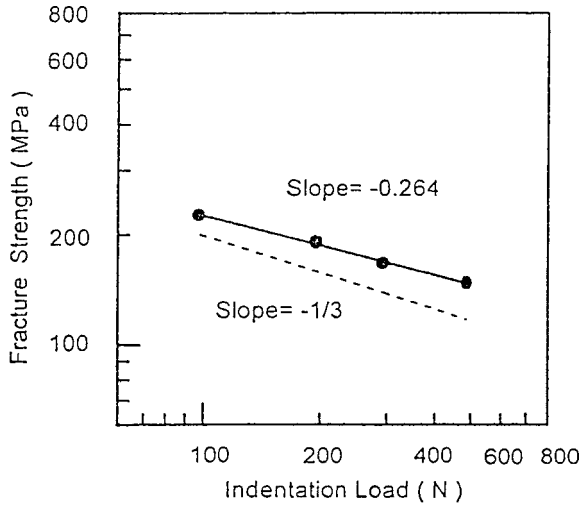

Figure 6 Variation in fracture strength versus indentation load in Al_2O_3-Cr_3C_2 composites.

toughness at large and small crack length limits was used to fit the measured R-curves as shown by the solid line [30].

Results in Fig. 5 indicate a trend of increasing fracture resistance as the crack extends. In addition, an upper-bound saturation fracture toughness was obtained at large crack lengths. Although there was some overlap in values, the toughness determined from instable cracks (open squares) appeared to be greater than that from the initial cracks at the same crack length (solid squares). This was probably due to the differences in tip radius and shape of crack front between the initial and instable cracks [31].

3.3.2. Indentation strength in bending (ISB)

Plots of flexural strength (σ) as a function of indentation load (P) are shown in Fig. 6. The slopes of initiation crack length versus indentation load can also be determined. The fracture toughness at various crack length can therefore be calculated from Equations 1–5 as shown in Fig. 7. The toughness appeared to be constant for the monolithic alumina samples. The toughness of alumina increased substantially and R-curve behavior became quite evident however, after the incorporation of Cr_3C_2 particles.

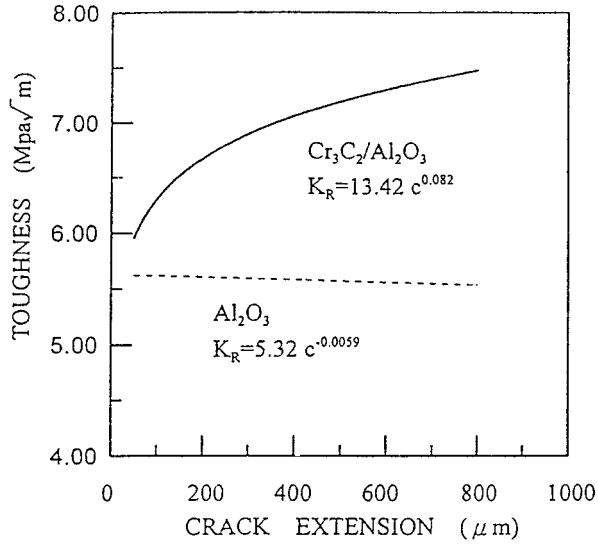

Figure 7 Plots of toughness versus crack length determined by indentation strength in bending (ISB) method.

4. Summary and conclusions

1. The time-dependent slow crack growth occurred in both alumina and an Al_2O_3-Cr_3C_2 composite under static fatigue test conditions.

2. Results from dynamic and static fatigue tests show that the resistance to slow crack growth in the Al_2O_3-Cr_3C_2 composite is higher than that in monolithic alumina.

3. The toughness of alumina was substantially increased and R-curve behavior became evident after the incorporation of Cr_3C_2 toughening particles.

Acknowledgment

The authors would like to thank the National Science Council, Republic of China, for its support under Grant No. NSC85-2216-E006-034.

References

1. C. T. FU, J. M. WU and A. K. LI, *J. Mater. Sci.* **29** (1994) 2671.
2. S. LIO. M. WATANABE, M. MATSUBARA and Y. MATSUO, *J. Amer. Ceram. Soc.* **72** (1989) 1880.
3. W. J. TSENG and P. D. FUNKENBUSCH, *ibid.* **75** (1992) 1171.
4. D. F. LII, J. L. HUANG, K. C. TWU and A. K. LI, *J. Ceram. Soc. Jpn.* **104** (1996).
5. J. L. HUANG, K. C. TWU, D. F. LII and A. K. LI, *J. Mater. Chem. and Phys.* **51** (1997) 211.
6. C. T. FU and J. M. WU, *J. Mater. Sci.* **29** (1994) 2617.
7. C. T. FU, A. K. LI and J. M. WU, *ibid.* **28** (1993) 6285.
8. K. M. SHU, C. T. FU and J. M. LIU, *J. Mater. Sci. Lett.* **13** (1994) 1146.
9. J. MATSUSHITA, H. NAGASHIMA and H. SAITO, *J. Ceram. Soc. Jpn.* **198** (1990) 452.
10. C. T. FU, A. K. LI and J. M. WU, *J. Mater. Sci.* **28** (1993) 6258.
11. J. L. HUANG, K. C. TWU, K. F. LII and A. K. LI, *J. Ceram. Soc. Jpn.* **104** (1996) 796.
12. R. F. KRAUSE, *J. Amer. Ceram. Soc.* **77** (1994) 72.
13. *Idem., ibid.* **71** (1998) 338.

14. J. C. NEWMAN and I. S. RAJU, *Engineering Fracture Mechanics* **15** (1981) 185.
15. R. F. COOK and B. R. LAWN, *J. Amer. Ceram. Soc.* **66** (1983) c-200.
16. R. M. ANDERSON and L. M. BRAIN, *ibid.* **73** (1990) 3059.
17. G. R. ANSTIS, P. CHANTIKUL, B. R. LAWN and D. B. MARSHALL, *ibid.* **64** (1981) 533.
18. D. BLEISE and R. W. STEINBRECH, *ibid.* **77** (1994) 315.
19. N. RAMACHANDRAN, L. CHAO and D. K. SHETTY, *ibid.* **76** (1993) 961.
20. C. W. LI and J. YAMANIS, *Ceram. Eng. Sci. Pro.* **10** (1989) 632.
21. J. E. RITTER, *Fracture Mechanics of Ceramics* **4** (1978) 667.
22. A. G. EVANS, *Int. J. Frac.* **10** (1974) 251.
23. J-L. HUANG, Ph.D. Dissertation, "Delayed Failure And High Speed Fracture of Ceramic Materials With Particular Emphasis on The Role of Interfaces," University of Utah (1984).
24. J. L. HUANG and J. M. JIH, *J. Mater. Res.* **10** (1995) 2488.
25. W. B. HILLING and R. J. CHARLES, in "High Strength Materials," edited by V. F. Zackay (John Wiley & Sons, New York, 1964), p. 682.
26. M. C. KNECHTEL, D. E. GARCIA, J. RODEL and N. CLAUSSEN *J. Amer. Ceram. Soc.* **76** (1993) 2681.
27. R. F. KRAUSE, JR. and E. R. FULLER, JR. *ibid.* **73** (1990) 559.
28. STANLEY M. SMITH and RONALD O. SCATTERGOOD, *J. Amer. Ceram. Soc.* **75** (1992) 305.
29. American Society For Testing and Materials Standard E740-80.
30. N. RAMACHANDRAN and D. K. SHETTY, *ibid.* **74** (1991) 2634.
31. M. S. KALISZEWSKI, G. BEHRENS, A. H. HEUER, M. C. SHAW, D. B. MARSHALL, G. W. DRANSMANN, R. W. STEINBRECH, A. PAJARES, F. GUIBERTEAU, F. L. CUMBRERA and A. DOMINGUEZ-RODRIGUEZ, *ibid.* **77** (1994) 1185.

Received 7 February
and accepted 31 December 2001